Supporting Information

A zinc bromine "supercapattery" system combining triple functions of capacitive, pseudocapacitive and battery-type charge storage

Feng Yu,[1‡] Chunmei Zhang,[1‡] Faxing Wang,[2] Yangyang Gu,[1] Panpan Zhang,[2] Eric. R. Waclawika,[1] Aijun Du,[1] Kostya (Ken) Ostrikov,[1] and Hongxia Wang*[1]

[1] School of Chemistry, Physics and Mechanical Engineering, Science and Engineering Faculty, Queensland University of Technology, Brisbane, QLD 4001, Australia

[2] Department of Chemistry and Food Chemistry & Center for Advancing Electronics Dresden (cfaed), Technische Universität Dresden, Dresden, 01062, Germany

Experimental section

Material synthesis. The porous sulfur and phosphorus co-doped carbon (S/P-C) was prepared by a simple carbonization method. First, MOF-5 sample was prepared according to the method reported in literature.[1] In brief, 18 mmol of $Zn(NO_3)_2$ and 6 mmol of Terephthalic acid (H_2BDC) were dissolved in 75 ml of Dimethyl formamide (DMF) solution, respectively. Afterwards, the two solutions were mixed in a beaker, and then heated at 120 ^oC for 8 h. After the reaction, the precipitate was washed thoroughly with DMF and absolute ethanol before being dried at 80 ^oC for 12 h. Second, 500 mg of MOF was uniformly dispersed in 60 mL of deionized (DI) water, and 1.2 mL of thioglycolic acid (TA) and 1.2 mL of phytic acid (PA) were mixed with MOF dispersion by ultrasonic treatment for 30 min, Then the as-prepared solutions were mixed and placed in oven at 80 ^oC for 10 h to dry. Finally, as prepared sample was then placed into a ceramic boat and annealed at 800 ^oC for 2 h under N_2 atmosphere using horizontal quartz tube furnace. The temperature of the furnace was slowly increased from room temperature to 800 ^oC with a heating rate of 3 ^oC min^{-1}. After the annealing, the sample was cooled naturally to room temperature before being used for further characterization.

The CC/Zn was prepared by an electrodeposition method, employing an electrochemical working station SP-150. In brief, a piece of carbon cloth was used as work electrode (1 cm × 2 cm) and precleaned by ultrasounding in ethyl alcohol for 15 min. 12.5 g zinc sulfate ($ZnSO_4 \cdot 7H_2O$),

12.5 g sodium sulfate (Na_2SO_4), and 2 g boric acid (H_3BO_3) was dissolved in 100 mL distilled water and used as electrolyte. The electrodeposition was conducted with a constant current density of −50 mA cm^{-2} for 10 min at room temperature.

Material characterization. X-ray diffraction (XRD) patterns were collected using a PAnaytical MPD equipped with Cu Ka radiation. Field emission Scanning electron microscopy (FESEM) was conducted on JSM-7001F equipped with energy dispersive X-ray spectroscopy (EDS) using an accelerating voltage of 20 kV. Nitrogen sorption–desorption isotherms were measured at 77 K using Micromeritics Tristar II 3020. Prior to the measurements, the samples were degassed under vacuum at 200 ^oC for 10 h. The Brunauer–Emmett–Teller (BET, Micromeritics 3Flex) method was utilized to calculate the specific surface areas (SBET). Using the Barrett–Joyner–Halenda (BJH) model, the pore volumes and size distributions were derived from the adsorption branches of the isotherms. Surface electronic states were obtained by X-ray photoelectron spectroscopy (XPS; Kratos AXIS Supra photoelectron spectrometer) using Al KR radiation, and the binding energy values were calibrated using the C1s of graphite at 284.6 eV as a reference.

Electrochemical measurement. For the anode, commercial carbon cloths (CCs) were treated in 6 M HNO_3 solution for 2 h with sonication to remove the impurities and endow the surface with hydrophilic groups. For the Zn ion electrodeposition tests, a standard three-electrode cell was used in the 0.5M K_2SO_4 and 1M $ZnSO_4$ hybrid electrolyte, which consists of the above CCs as the working electrode, a Pt wire as counter electrode and a saturated calomel electrode (SCE) as reference electrode. Then a two-electrode cell was employed to check the electrochemical activity of Zn@CCs electrodes in the hybrid electrolyte. For the cathode, the as-prepared S/P-C was mixed with acetylene black and poly(tetrafluoroethylene) (PTFE) in a weight ratio of 8:1:1, respectively, with the help of ethanol. After drying, the mixture was pressed into a film, and then the film was cut into disks with the area of 1 cm^2 and the mass of 2 mg. These disks were pressed onto graphite rod to act as electrodes after drying at 120 ^oC overnight. The half -cell tests of S/P-C electrode in the 0.5M K_2SO_4 and 1M KBr hybrid electrolyte were carried out in the standard three-electrode cell consisting of the S/P-C as the working electrode, a graphite rod as counter electrode and a saturated calomel electrode (SCE) as reference electrode. For the full-cell tests, the S/P-C as the cathode and the CCs as the anode was assembled in a two-electrode cell using the above hybrid solution as the electrolyte and the Nafion film as the separator. The cyclic voltammetry (CV) data

were collected on an electrochemical working station SP-150 (BioLogic Science Instruments). The galvanostatic charge-discharge (GCD) data was obtained on the LAND battery test systems. All tests were carried out at room temperature.

Computational Methods. The calculations were performed using density functional theory (DFT) methods within generalized gradient approximation of the Perdew−Burke−Ernzerhof (PBE) functional, as implemented in the Vienna ab initio simulation package (VASP).[2–4] For calculations charge density difference of the Br/AC, Br/ACS_2, Br/ACP_2 and Br/ACSP, we choose the monolayer graphene with 4×4×1 supercell to simulate AC. A dispersion correction of total energy (DFT-D3 method) was used to incorporate the long-range vdW interaction. To study 2D systems under the periodic boundary condition, a vacuum layer with a thickness 10 Å and a plane-wave basis set with an energy cut-off of 500 eV was set to minimize artificial interactions between neighbouring layers. The structures studied here were fully relaxed until energy and force converged to 10^{-6} eV and 0.001eV/Å, respectively. The adsorption energies of Br on AC is calculated based on the following equation[5]

$$E_b = E_{ACBr\_} E_{AC} - E_{Br} \qquad (equa.\ 1)$$

Where E_{Br} is the cohesive energy of the Br atom, and E_{AC} and E_{ACBr} are the total energies of AC nanosheet before and after Br adsorption.

For calculations energy diffuse barrier of graphene/Zn and graphene, the square supercell of 3x5x1 graphene and graphene with two layers Zn (3x5x1 supercell) (gra/Zn) were used for studying Zn adsorption and diffusion. The Zn intercalated graphene and gra/Zn systems were relaxed until energy and force were converged to 10-6 eV and 0.001eV/Å, respectively. The climbing image nudged elastic band (NEB) 5-6 method was used for finding saddle points and the minimum energy path.

Supporting Figures

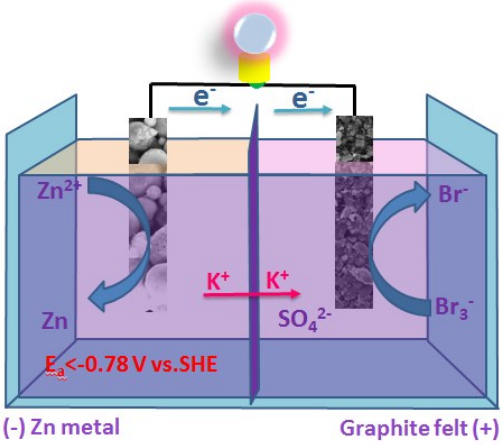

Fig. S1 Schematic illustration of the working principle of aqueous Zn-Br_2 battery at discharge process. There are not electrical-double-layer (EDL) type and pseudocapacitive charge storage in the anode and cathode. In addition, during the charging process of the aqueous Zn-Br_2 battery, the Zn^{2+} electrodeposition occurs below the potential of -0.78V vs. SHE.

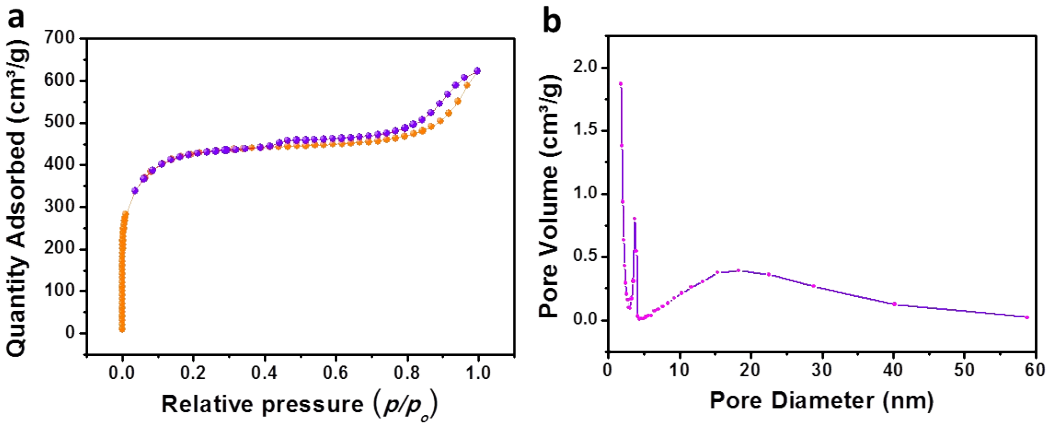

Fig. S2 (a) The nitrogen adsorption-desorption isotherms and (b) the corresponding pore size distribution curve of the S/P-C.

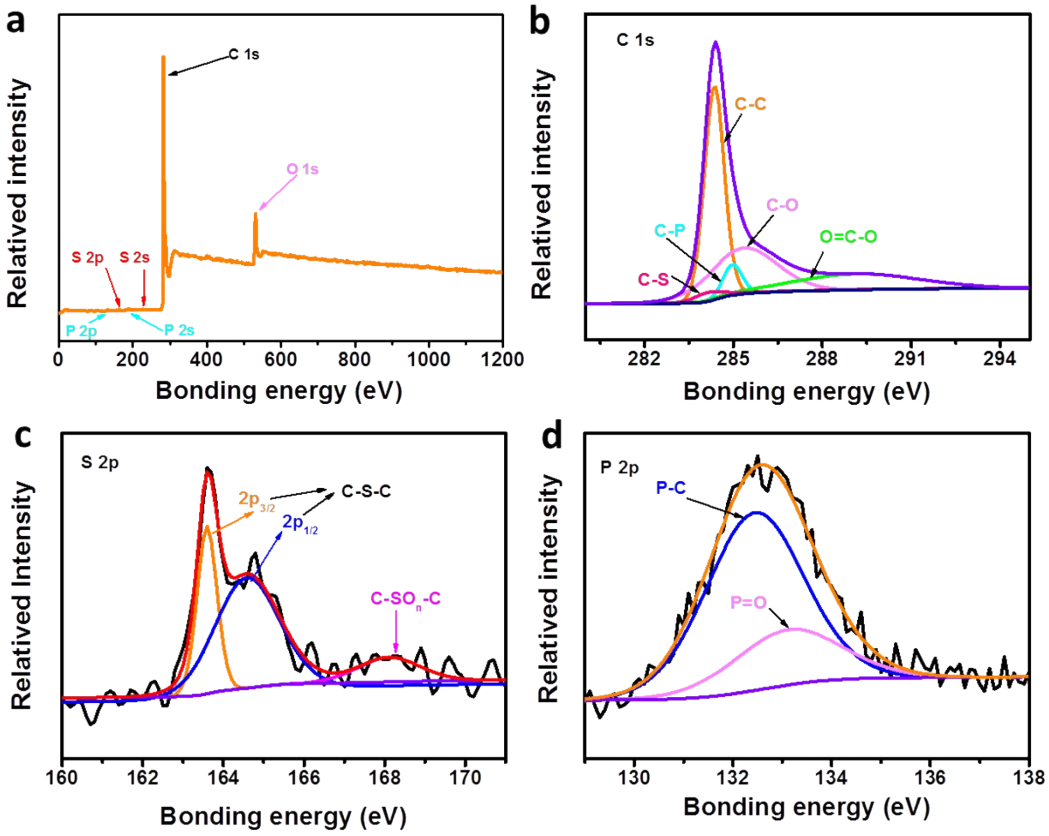

Fig. S3 XPS analysis of (a) the S/P-C, and the corresponding (b) C-1s peak, (c) S-2p peak, (d) P-2p peak.

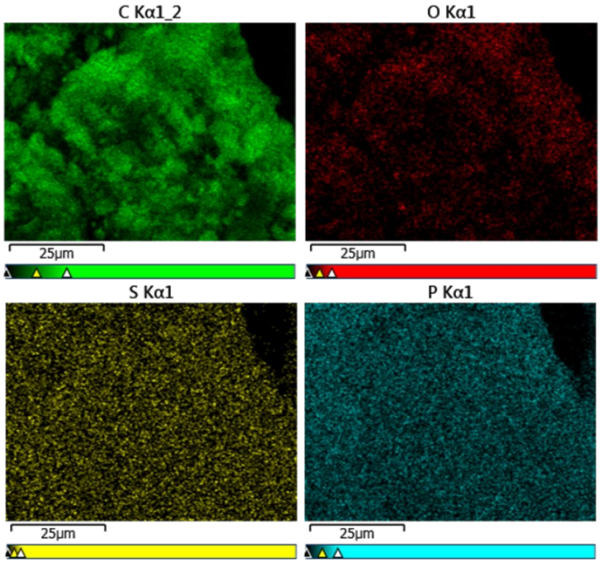

Fig. S4 The EDX element mapping analysis of the S/P-C.

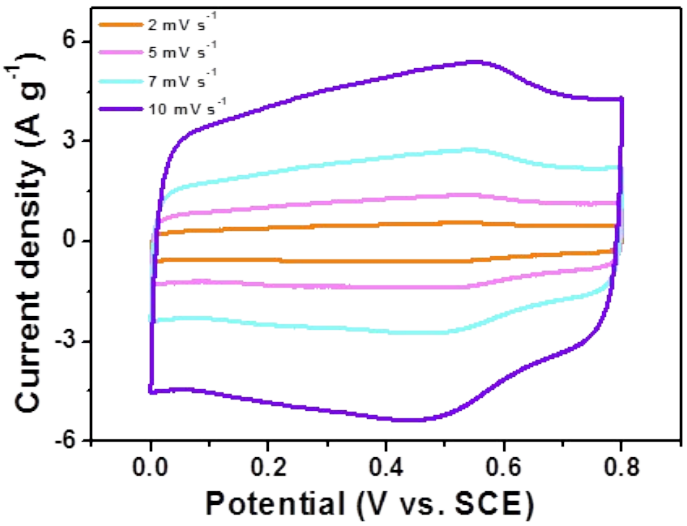

Fig. S5 The CV curves of the S/P-C electrode in the electrolyte without KBr additive at various scan rates.

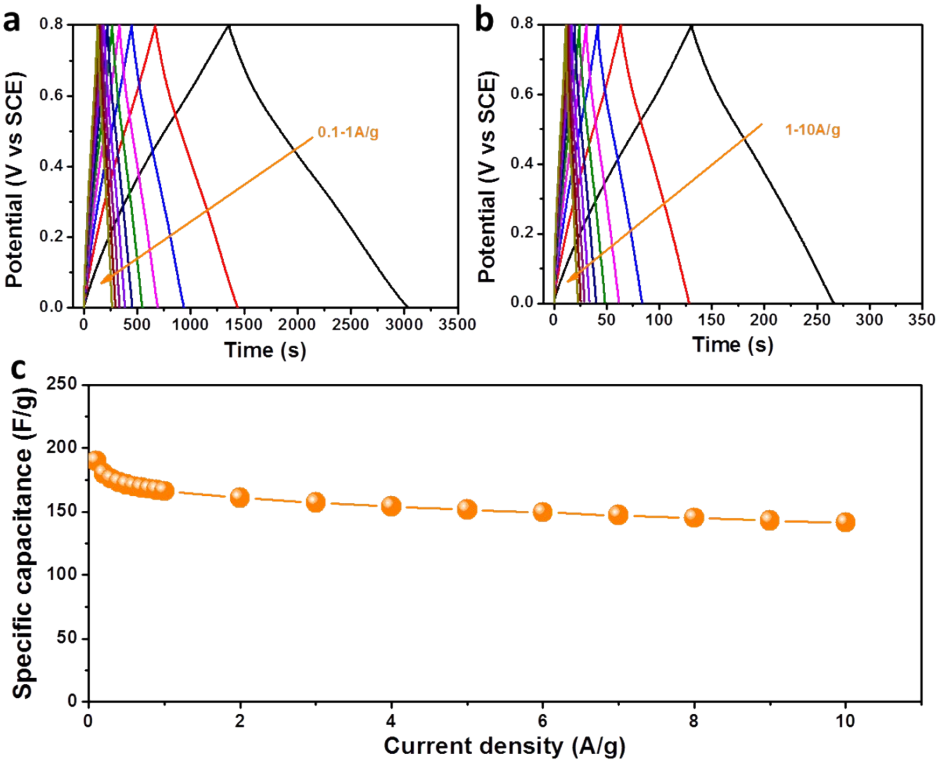

Fig. S6 The charge/discharge curves of the S/P-C electrode in the electrolyte without KBr additive at the current density ranges of (a) 0.1−1 A g^{-1} and (b) 1−10 A g^{-1}. (c) The calculated specific capacitances at the above various current densities.

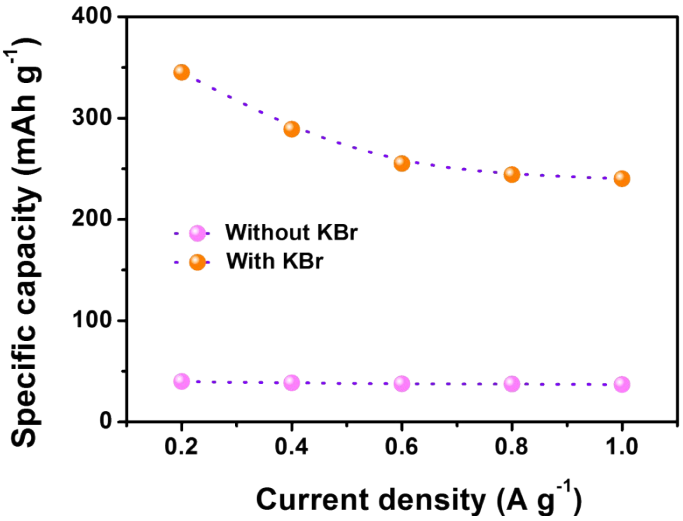

Fig. S7 The specific capacities of S/P-C electrode in the hybrid electrolyte with and without the KBr additive.

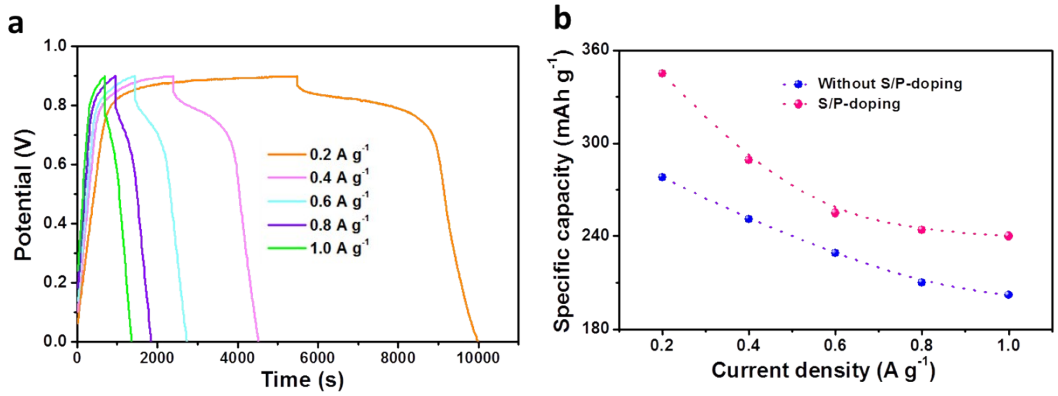

Fig. S8 (a) The GCD curves of the porous carbon without any heteroatoms synthesized by the same method in the electrolytes with 1M KBr redox additive. (b) The comparison of the specific capacities of the S/P-C electrodes and the porous carbon without any heteroatoms at various current densities.

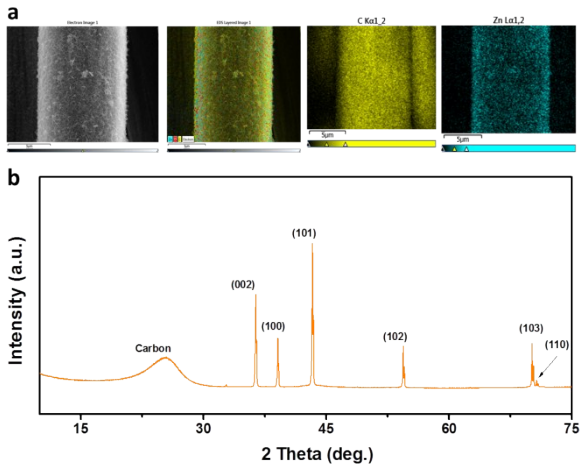

Fig. S9 (a) The EDX element mapping analysis and (b) the XRD patterns of Zn@CCs.

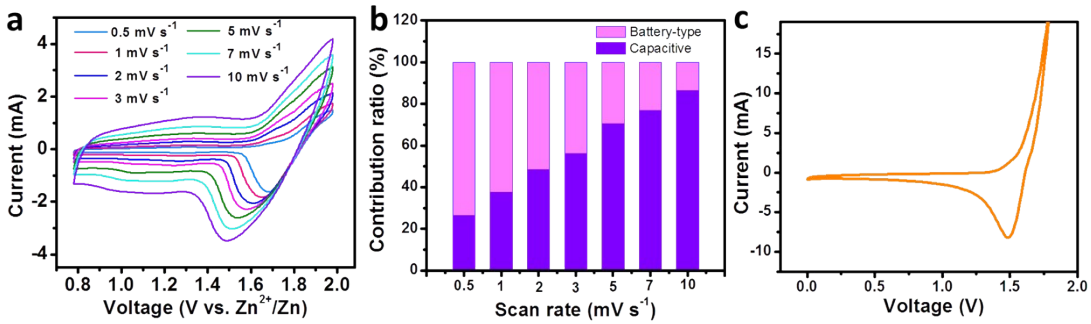

Fig. S10 (a) The CV curves of the Zn-Br_2 supercapattery. Below the voltage of 1.3V, the charge storage is mainly from capacitive contributions. (b) The identified contribution ratios of capacity from the capacitive processes and diffusion-controlled (battery-type) process. the quantitative contribution of the capacitive and battery-type charge storage was obtained using the equation of $i = k_1v + k_2v^{1/2}$, where i, v, k_1v, and $k_2v^{1/2}$ represent the total current at a specific potential, scan rate, capacitive current, and diffusion-controlled (battery-type) current, respectively.[5–9] (c) The curve of the Zn-Br_2 battery at 10 mV s^{-1}. There are almost no capacitive contributions especially in the voltage range of 0−1.3 V.

At 0.5 mV s^{-1} (3900 seconds for the cathodic or anodic processes), the calculated capacitive contribution of the Zn-Br_2 supercapattery was approximately 26% (Fig. S10b). When the scan rate incases to 10 mV s^{-1} (195 seconds for the cathodic or anodic processes), the capacitive contribution reaches up to 82%. Notably, for the $3Br^-/Br_3^-$ redox reaction, it is now widely recognized that the bromine ions reacting on the surface of the carbon current densities without pores (like carbon felts for redox flow batteries) are based on the battery-type redox reaction [10,11] while those bromine ions confined in porous carbon electrodes produce pseudocapacitances.[12,13] Unfortunately, for our S/P co-doped carbon, it is hard to make quantitative distinctions between pseudocapacitive contribution from Br^-/Br_3^- and battery-type contribution from Br^-/Br_3^- because the porous S/P co-doped carbon has extra EDL capacitance and pseudocapacitances.

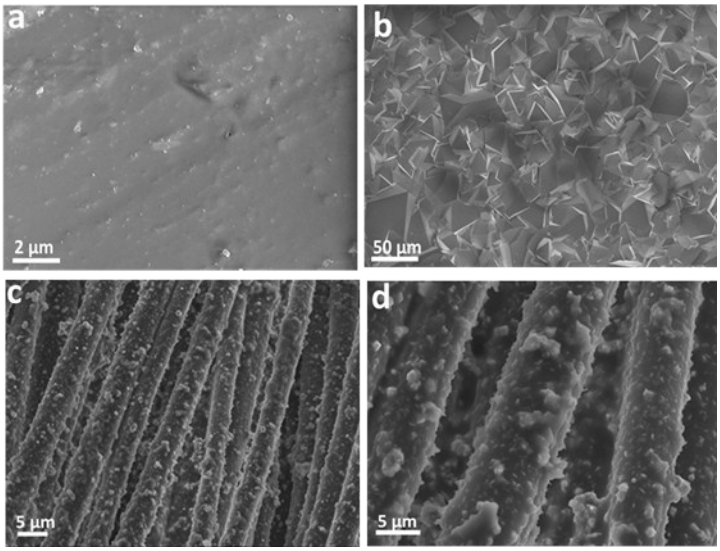

Fig. S11 (a) The SEM image pure Zn anode before cycles. (b) The SEM image of the pure Zn anode after 5000 cycles. (c, d) The SEM images of the Zn@CCs anode after 5000 cycles.

After repeated cycles, the uncontrolled Zn dendrite growth is clear for pure Zn electrode along the vertical direction. However, compared with the pure Zn anode, the dendrite growth for Zn@CCs andeo after 5000 cycles was effectively suppressed.

Table S1. The comparison of working voltage, power/energy densities, and cycle lifespans among the state-of-the-art aqueous Zn-ion batteries, the redox-additive-enhanced supercapacitors and our Zn-Br_2 supercapattery with EDL-type, pseudocapacitive and battery-like charge storage in both cathode and anode.

Electrodes (-)//(+)	**Voltage**	**Energy density (corresponding power density)**	**Cycles**	**Ref.**
Zn//$ZnMn_2O_4$@C	0.8-1.9V	202 Wh kg^{-1} (<1000 W kg^{-1})	500 (94%)	14
Zn//$Zn_{0.25}V_2O_5{\cdot}nH_2O$	0.5-1.4V	~202 Wh kg^{-1} (~5500 W kg^{-1})	1000 (81%)	15
Zn//VS_2	0.4-1.0V	123 Wh kg^{-1} (<1500 W kg^{-1})	200 (98%)	16
Zn//$H_2V_3O_8$@graphene	0.2-1.6V	168 Wh kg^{-1} (34 W kg^{-1})	2000 (100%)	17
Zn//$Zn_3V_2O_7(OH)_2{\cdot}2H_2O$	0.2-1.8V	~200 Wh kg^{-1} (~300 W kg^{-1})	300 (68%)	18
Zn//$Ca_{0.25}V_2O_5{\cdot}nH_2O$	0.6-1.6V	133 Wh kg^{-1} (1825 W kg^{-1})	3000 (96%)	19
Zn//$Na_2V_6O_{16}{\cdot}3H_2O$	0.4-1.4V	138 Wh kg^{-1} (7900 W kg^{-1})	1000 (100%)	20
Zn//Br_2	0.2-1.9V	144 Wh kg^{-1} (<3000 W kg^{-1})	1000 (100%)	21
MV^{2+}/MV^{+}// Br^{-}/Br_3^{-}	0-1.4V	~110 Wh kg^{-1} (<150 W kg^{-1})	2000 (100%)	12
HV^{2+}/HV^{+}// Br^{-}/Br_3^{-}	0-1.2V	[a] 48 Wh kg^{-1} (2000 W kg^{-1})	10000 (100%)	22
EV^{2+}/EV^{+}// Br^{-}/Br_3^{-}	0-1.3 V	[a] 64 Wh kg^{-1} (3000 W kg^{-1})	7000 (96%)	13
Zn@CC// Br^{-}/Br_3^{-}@S,P-C	0-1.8V	181Wh kg^{-1} (9300 W kg^{-1}) [a] ~60 Wh kg^{-1} [a] (~3000 W kg^{-1})	5000 (81%)	This work

For all the listed Zn-ion batteries, the mass of the used electrolytes was excluded from the calculation of values of energy density and power density. [a] The values were obtained based on the total mass of active electrode and the used electrolyte.

References

(1) F. Yu, T. Wang, Z. Wen and H. Wang, *J. Power Sources*, 2017, **364,** 9.

(2) S. Grimme, *J. Comput. Chem.*, 2006, **27**, 1787.

(3) G. Henkelman and H. Jónsson, *J. Chem. Phys.*, 2000**, 113**, 9978.

(4) C. Zhang, Y. Jiao, T. He, F. Ma, L. Kou, T. Liao, S. Bottle and A. Du, *Phys. Chem. Phys. Chem*., 2017, **19**, 25886.

(6) T. Brezesinski, J. Wang, S. H. Tolbert and B. Dunn, *Nat. Mater.*, 2010, **9**, 146.

(7) C. Chen1, Y. Wen, X. Hu, X. Ji, M. Yan, L. Mai, P. Hu, B. Shan and Y. Huang, *Nat. Commun.*, 2015, **6**, 6929.

(8) H. S. Kim, J. B. Cook, H. Lin, J. S. Ko, S. H. Tolbert, V. Ozolins and B. Dunn, *Nat. Mater.*, 2017, **16**, 454.

(9) C. Xia, J. Guo, P. Li, X. Zhang and H. N. Alshareef, *Angew. Chem. Int. Ed.*, 2018, **57**, 3943.

(10) S. Suresh, M. Ulaganathan and R. Pitchai, *J. Power Sources*, 2019, DOI: https://doi.org/10.1016/j.jpowsour.2019.226998.

(11) L. Zhang, Q. Lai, J. Zhang and H. Zhang, *ChemSusChem*, 2012, **5**, 867−869.

(12) S. E. Chun, B. Evanko, X. Wang, D. Vonlanthen, X. Ji, G. D. Stucky and S. W. Boettcher, *Nat. Commun.*, 2015, 6, 7818.

(13) S. J. Yoo, B. Evanko, X. Wang, M. Romelczyk, A. Taylor, X. Ji, S. W. Boettcher and G. D. Stucky, *J. Am. Chem. Soc.*, 2017, **139**, 9985.

(14) N. Zhang, F. Cheng, Y. Liu, Q. Zhao, K. Lei, C. Chen, X. Liu, J. Chen, *J. Am. Chem. Soc.*, 2016, **138**, 12894.

(15) D. Kundu, B. D. Adams, V. Duffort, S. H. Vajargah and L. F. Nazar, *Nat. Energy*, 2016, **1**, 16119.

(16) P. He, M. Yan, G. Zhang, R. Sun, L. Chen, Q. An and L. Mai, *Adv. Energy Mater*., 2017, **7**, 1601920.

(17) Q. Pang, C. Sun, Y. Yu, K. Zhao, Z. Zhang, P. M. Voyles, G. Chen, Y. Wei and X. Wang, *Adv. Energy Mater*., 2018, **8**, 1800144.

(18) C. Xia, J. Guo, Y. Lei, H. Liang, C. Zhao and H. N. Alshareef, *Adv. Mater*., 2018, **30**, 1705580.

(19) C. Xia, J. Guo, P. Li, X. Zhang and H. N. Alshareef, *Angew. Chem. Int. Ed*., 2018, **57**, 3943.

(20) V. Soundharrajan, B. Sambandam, S. Kim, M. H. Alfaruqi, D. Y. Putro, J. Jo, S. Kim, V. Mathew, Y. K. Sun and J. Kim, *Nano Lett*., 2018, **18**, 2402.

(21) S. Biswas, A. Senju, R. Mohr, T. Hodson, N. Karthikeyan, K. W. Knehr, A. G. Hsieh, X. Yang, B. E. Koel and D. A. Steingart, *Energy Environ. Sci*., 2017, **10**, 114.

(22) B. Evanko, S. J. Yoo, S. E. Chun, X. Wang, X. Ji, S. W. Boettcher and G. D. Stucky, *J. Am. Chem. Soc.*, 2016**, 138**, 9373.